Numerical and Experimental investigation of the stability of the 3D flow between two counter–rotating disks

Olivier Daube[1], Patrick Le Quéré[2], Frédéric Moisy[3], and Marc Rabaud[3]

[1] CEMIF/LME, Université d'Evry, 91020 Evry Cedex, France
[2] LIMSI-CNRS, BP 133, 91403 Orsay Cedex, France
[3] FAST, Bât 502, Université Paris Sud, 91405 Orsay Cedex, France

Abstract. This paper is devoted to a numerical and experimental study of the 3D flow in a cylindrical cavity of large radius-to-height aspect ratio whose top and bottom lids are rotating in opposite directions. This counter rotation gives rise to a new type of instability pattern, referred as negative spirals. Comparisons between numerical and experimental results give evidence that a free shear layer instability is responsible for this new pattern.

1 Introduction

The flows between rotating disks, or von Kármán swirling flows, occur in a variety of situations, and have been studied since a long time. The stability of these flows received considerable interest, mostly in the rotor-stator configuration [5,6,2] (i.e. between one rotating disk and one stationary disk), and it is only recently that 3D numerical simulations for moderate radius-to-height aspect ratio $\Gamma = R_0/H$ became available [7]. These studies focused on the boundary layer instabilities, leading to spiral or circular waves.

In this study, it is shown that in the case of counter–rotating disks, another type of instability may also occur. The pattern associated to this new instability received the name of negative spirals [3], since they roll up to the center in the direction of the slower disk. Similar patterns have been reported for smaller aspect ratio, $\Gamma = 2$ [11], and were attributed to a free shear layer instability. The influence of the aspect ratio have been recently studied experimentally [4].

The configuration is defined in figure 1. The flow is characterized by three non dimensional parameters:

$$\mathrm{Re}_t = \frac{\Omega_t H^2}{\nu} \; ; \; \mathrm{Re}_b = \frac{\Omega_b H^2}{\nu} \; ; \; \Gamma = \frac{R_0}{H}.$$

The set of parameters $(\mathrm{Re}_t, s, \Gamma)$ may be also used for convenience, where $s = \Omega_b/\Omega_t$ is the counter-rotation ratio ($|s| < 1$ in the present study).

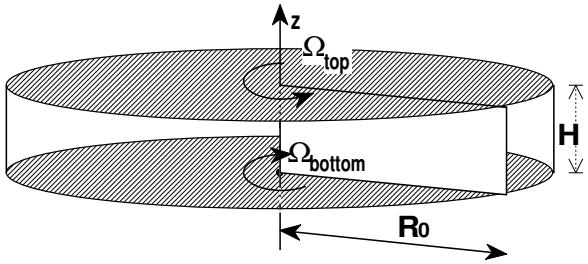

Fig. 1. Geometry of the flow between rotating disks. The lateral endwall rotates with the upper disk.

2 The numerical method

The numerical method is described in [8] and has the following main ingredients:
Time discretization: A second order time marching procedure is used with an implicit discretization of the linear terms and an explicit Adams-Bashforth type extrapolation of the non linear terms. In the resulting discrete problem to be solved at each time step, the velocity–pressure coupling is handled by means of an incremental projection method [10].
Spatial discretization: In the previously time discretized system, the different unknowns are first expanded in truncated Fourier series over N modes in the azimuthal direction. The coefficients of this expansion are discretized in the (r, z) planes by means of mimetic finite difference operators [9]:

- A classical staggered uniform grid in cylindrical coordinates (r, θ, z) is used. Noteworthy is the fact that the only unknown located on the axis $r = 0$, is the axial component ζ of the vorticity.
- The space $\mathcal{H}$ of the discrete vectors and the space H of the discrete scalar functions are equipped with inner products $<,>_{\mathcal{H}}$ and $<,>_{\mathrm{H}}$ derived from the $\mathbb{L}^2$ inner products of the continuum case,
- The first order differential operators divergence and curl, are discretized by means of the Gauss and Stokes theorems written on elementary cells,
- The discrete gradient operator is defined as the negative adjoint of the discrete divergence operator with respect to the discrete inner products.
- The second order differential operators are built as compounds of first order discrete operators, therefore ensuring that the Laplace operators are self adjoint. This fact, together with the use of a staggered grid, ensures that the discrete problem to be solved at each time step is well posed,
- The non linear terms are written as $(\nabla \times \boldsymbol{v}) \times \boldsymbol{v}$ and discretized in order that $< \boldsymbol{v}\,, (\nabla \times \boldsymbol{v}) \times \boldsymbol{v} >_{\mathcal{H}} = 0$, therefore ensuring kinetic energy conservation. As usual, they are computed in the physical space with the classical 3/2 rule.

3 Experimental results

The experimental set-up, described in detail in Ref. [3,4], consists in a rotating cylinder of radius $R = 140$ mm, in which a disk of same radius rotates at a different speed. In this paper we are only concerned with the counter-rotation case, where the faster disk is the top one ($|\Omega_t| \geq |\Omega_b|$). The working fluid is a mixture of water and glycerol of kinematic viscosity lying in the range $1.0 \times 10^{-6} < \nu < 4 \times 10^{-6}$ m^2/s at 20^{o}C. Qualitative insight of the flow structure is obtained from visualization of the light reflected by anisotropic flakes seeding the flow (Kalliroscope). The flow is illuminated by a concentric circular light source, and pictures are obtained using a CCD camera located along the disks axis.

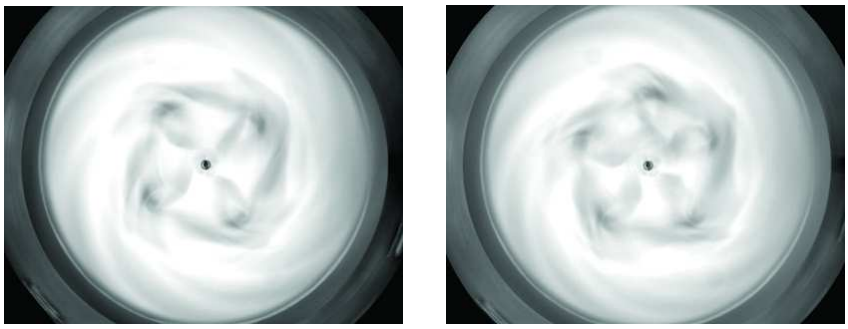

(a) (b)

Fig. 2. Examples of patterns observed between rotating disks. (a) $m = 4$, (b) $m = 5$.

At high enough Reynolds numbers, the counter-rotating flow gives rise to instability patterns such as the ones shown in figure 2. They consist in a circular chain of vortices surrounded by a set of spirals (negative spirals [3]). Depending on the mode and the aspect ratio, only the circular chain of eddies or the negative spirals may be observed. High aspect ratios R/h and/or low mode essentially leads to eddies, while lower aspect ratios and/or higher modes mostly show negative spirals. Intermediate modes, roughly between 4 and 7, usually shows a combination of the two aspects of the pattern.

The stability curve of these patterns is shown in figure 3 for different aspect ratios. These curves are obtained by slowly increasing the bottom disk angular velocity Ω_b at fixed value of Ω_t. No hysteresis is observed within our experimental uncertainty, around 3%. When plotted as functions of the Reynolds numbers ($\Gamma Re_t, \Gamma Re_b$), the different curves appear to collapse into a single master curve. The fact that the chain of vortices and negative spirals share the same onset curve indicate that they both arise from the same instability mechanism, although the nonlinear saturation leads to very different morphology. We note that at high Reynolds number, the onset is well

described by a single non dimensional parameter, the counter-rotation ratio

$$s = \frac{Re_b}{Re_t} \simeq -0.135 \pm 0.010.$$

However, at lower Reynolds numbers, this linear curve appears to saturate towards a finite bottom Reynolds number,

$$\Gamma Re_b \simeq -230 \pm 20.$$

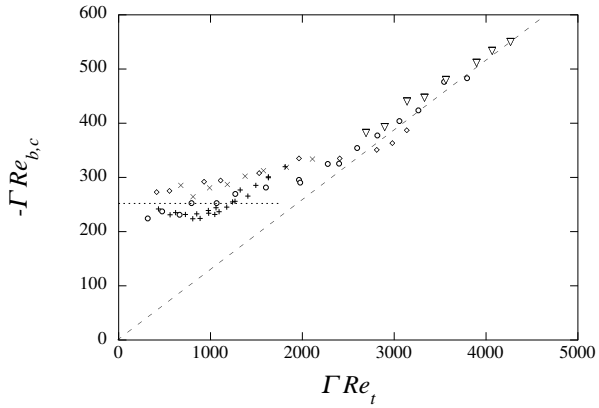

Fig. 3. Stability curve of negative spirals for aspect ratios $\Gamma = R/h = 6.1$ (∇), 7.0 (o), 10.8 ($\diamond$), 14.0 ($\times$) and 20.9 ($+$).

The collapse of the curves for different aspect ratios gives indication for the mechanism responsible of the instability, because the shear and the boundary layers behave differently when R/h is varied. Assuming that the growth rate is controlled by the shear $S \sim \Omega R/h$, damped by viscous diffusion on a time scale $\tau_v \sim h^2/\nu$, this leads to the natural control parameter $S\tau_v = \Omega Rh/\nu = \Gamma Re$. So the master curve obtained in figure 3 suggests that a shear layer instability is responsible for the different patterns observed in figure 2.

4 Numerical results

The numerical results reported here have been obtained for $\Gamma = 7$, $s = -0.14$ and $\mathrm{Re}_t = 250$ on a 400×100 grid in the (r, z) variables and 32 Fourier modes in the azimuthal direction. The time step was taken equal to $1/500$ revolution time. In figure 4, contours in the plane $z = H/2$ of the axial velocity component are shown for $\Gamma = 7$; $\Gamma \mathrm{Re}_t = 1750$; $\Gamma \mathrm{Re}_b = 260$. The essential features of the experiments are recovered: existence of a mode $m = 4$ with surrounding negative spirals. Other calculations for a slightly different Re_b

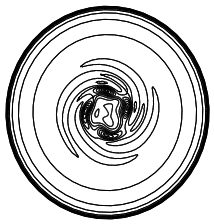

Fig. 4. Contours of the axial velocity component in the plane $z = 0.2H$; $\Gamma = 7$; $\mathrm{Re}_t = 250$; $\mathrm{Re}_b = 37$

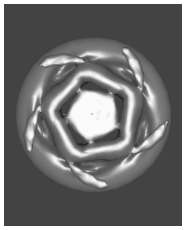

Fig. 5. Isosurface $w = 0.0354$ of the axial velocity ; $\Gamma = 7$; $\mathrm{Re}_t = 250$; $\mathrm{Re}_b = 41$

have been performed, showing the existence of a dominant $m = 5$ mode (see figure 5). Additional calculations (not reported here) have shown that for a further decrease of Re_b down to 252, the flow reverts to a steady axisymmetric regime, in excellent agreement with the experimental stability curve in figure 3.

Further insight into the mechanism of this instability can be achieved from these computations. As first noted by [1], at high enough counter-rotation ratio (roughly $|s| > 0.1$), the meridional flow gets organized into a two-cell recirculating flow. The competition between the centrifugal effects of each disk leads to the formation of a stagnation ring on the slower disk. This important property of the counter-rotation regime can be shown in figure 6: the sign of the azimuthal vorticity over the slower disk ($z = 0$) changes at $r/R_0 \simeq 0.36$.

The presence of this stagnation ring as important consequence on the azimuthal component of the flow, as shown in figure 7. For large radius, the shear layer between the positive velocity (associated to the faster disk) and the negative velocity (slower disk) remains within the inward boundary layer over the slower disk. At smaller radius, $r < 0.25R_0$, this shear layer gets detached because of the stagnation ring, leading to a free shear layer in the bulk of the flow. This phenomenon can be further seen in figure 6, where the location of the stagnation ring appears to coincide with the maximum of vertical vorticity. At high enough Reynolds number, this free shear layer may become unstable, leading to the instability patterns shown above.

Conclusion

The existence and onset of negative spirals have been confirmed both experimentally and numerically. Unlike other instabilities that are reported in the literature for this flow configuration, this new pattern is not associated to a boundary layer instability. Evidence is given that a free shear layer instability is responsible for this new pattern, in agreement with Ref. [11]. Additional experiments and computations (to be shown at the conference) show that

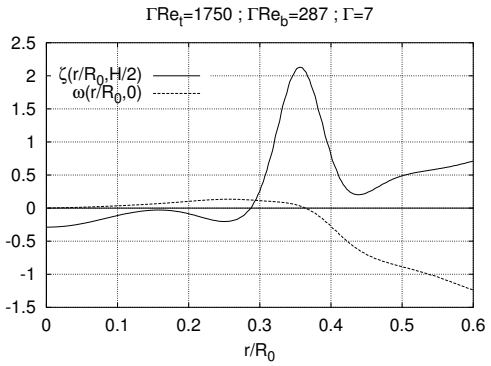

Fig. 6. Azimuthal vorticity along the slower disk $z = 0$ (dashed line) and vertical vorticity at mid-height $z = H/2$ (solid line).

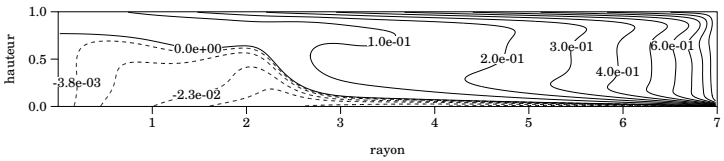

Fig. 7. Contours of the azimuthal velocity in the steady axisymmetric state.

modes with increasing wave number appear as the radius-to-height ratio is increased.

References

1. Dijkstra, D. and van Heijst, G.J.F., J. Fluid Mech. *128*, 123–154 (1983).
2. Gauthier, G., Gondret, P. and Rabaud, M., J. Fluid Mech. *386*, 105–126 (1999).
3. Gauthier, G., Gondret, P., Moisy, F. and Rabaud, M., J. Fluid Mech., in press (2002).
4. Moisy, F., Pasutto, T. and Rabaud, M., to appear in "Nonlinear Processes in Geophysics", Ed. W.G.Früh, (2002).
5. A.J. Faller, R.E. Kaylor, *Dynamics of Fluids and Plasmas*, Academic Press (1966).
6. L. Schouveiler, P. Le Gal, M.P. Chauve, J. Fluid Mech. *443* (2001).
7. E.Serre, E. Crespo del Arco, P. Bontoux, J. Fluid Mech. *434*, 65–100 (2001).
8. E. Barbosa, O. Daube, A Finite Differences Method in Cylindrical Coordinates for 3D Incompressible Flows, *ECCOMAS CFD Conference*, Swansea, UK (2001).
9. J.M. Hyman, M. Shashkov, Comp. Math. Appl. *33*, (1997).
10. K. Goda, J. Comp. Phys. *30* (1979).
11. J.M. Lopez, J.E. Hart, F. Marques, S. Kittelman, J. Shen, J. Fluid Mech. *462*, 383–409 (2002).